Research Article GU J Sci 38(3): 1388-1402 (2025) DOI: 10.35378/gujs.1553238

Gazi University

Journal of Science

http://dergipark.org.tr/gujs

First-Principles Study of Electronic and Magnetic Properties of Cr-, Fe-, and Ni-Doped ZnSe Supercells

Vusala JAFAROVA[1,2,*], Vusala EMINOVA[3,2], Nermin HASHIMOVA[1]

[1]*Azerbaijan State Oil and Industry University, 20 Azadlig Avenue, AZ-1010, Baku, Azerbaijan*
[2]*Khazar University, 41 Mehseti Street, AZ1096, Baku, Azerbaijan*
[3]*French-Azerbaijani University (UFAZ) under Azerbaijan State Oil and Industry University, 183 Nizami Street, AZ-1010, Baku, Azerbaijan*

Highlights

- Magnetization depends on concentration.
- FM phase is favored.
- HMFM with higher Curie temperature.

Article Info

Received: 20 Sep 2024
Accepted: 20 May 2025

Keywords

Curie temperature
Magnetic properties
Ferromagnetic
Antiferromagnetic
Simulations

Abstract

The magnetic behaviors in the ZnSe doped with 3d transition metal elements were analyzed. Analysis of electronic structures of $Zn_{1-x}TM_xSe$ systems shows additional peaks at the Fermi level derived from TM^{2+} 3*d* orbitals. The computed magnetic moments of approximately 4.0 μ_B for $Zn_{1-x}Cr_xSe$, $Zn_{1-x}Fe_xSe$, and $Zn_{1-x}Ni_xSe$ systems at impurity concentrations of x=6.25 % and 12.5 % indicate significant magnetic behavior and primary contribution to the magnetization of defective structures arising from the TM d states. Total energy simulations comparing ferromagnetic and antiferromagnetic behaviors demonstrate the ferromagnetic (FM) phase stability of ZnSe:(Cr, Fe, Ni). The magnetization of $TM_xZn_{1-x}Se$ systems is depends on the dopant concentration. Besides, Curie temperatures for ZnSe:TM systems were estimated and our results revealing that $Cr_xZn_{1-x}Se$ and $Ni_xZn_{1-x}Se$ compounds are promising candidates for spintronic applications such as spin valves, while $Fe_xZn_{1-x}Se$ is paramagnetic and represents a useful material for optoelectronics field.

1. INTRODUCTION

Nowadays, diluted magnetic semiconductor materials (DMSMs) have recently opened new avenues for the development of spin-based devices that combine high-speed performance with low energy consumption compared to traditional electronics. These materials pave the way for innovative technologies with major applications in both optoelectronics and spintronics.

Zn-based semiconductors from the II-VI group are among the most important and promising compounds due to their wide band gap, making them some of the best diluted magnetic semiconductors (DMSs). Higher Curie temperatures (T_C>300 K) in defective magnetic materials represent key emerging challenges in magnetism. DMSs find technical applications in spintronics primarily when doped with impurities. In particular, TM-doped systems demonstrate both ferromagnetic and half-metallic behaviors. These compounds have garnered considerable research attention for their potential in enabling efficient next-generation devices. Defective materials hold significant potential for quantum simulation architectures that utilize spin polarized electrons, as well as for magnetooptic applications.

3d metal (TM=Cr, Fe, Ni) doped II-VI group materials are promising compounds for fabrication of devices [1]. Recent advancements in DMMs demonstrate magnificent physical and chemical properties, which have great potential for application in spintronics [2-8]. An earlier research demonstrated $Mn_xZn_{1-x}Se$

*Corresponding author, e-mail: vusala.cafarova@asoiu.edu.az

could serve as a promising material for applications, particularly with the introduction of additional metal dopants [9]. Refs. [10-13] found the chromium doping in II-VI group compounds originates from ferromagnetic (FM) compounds. Ref. [14] reported results of measurements for the $(Cr, V)_xZn_{1-x}Se$ with cubic structures at x=4.5 % concentrations below 60 K and in $Zn_{1-x}V_xSe$ (at x=10 %) dopant ions dissolved in these systems. Ref. [14] reported that antiferromagnetic (AFM) phase correlations occur in $Cr_xZn_{1-x}Se$ at concentration of 15 %. Ref. [15] reported semi-metallic ferromagnetic (SMFM) behavior in $Cr_xZn_{1-x}Se$ systems, observing stability of the FM state. The literature review indicates a lack of conclusive results on the origin of magnetism in $Fe_xZn_{1-x}Se$. Iron-doped $Fe_xZn_{1-x}Se$ bulk solutions exhibit para-magnetic (PM) behavior at low temperatures [16, 17], while theoretical predictions suggest the possibility of FM and spin-glass (SG) behaviors [18], as well as AFM, PM, and SG phases [19].

ZnSe is a II-VI group, non-magnetic semiconductor with a wide bandgap (E_g=2.70 eV), making it a valuable material for technical applications across various fields [20]. Defective bulk solutions have attracted significant research interest for their potential in next-generation technical applications [21]. Ref. [12] found Curie temperatures of $(Cr, V)_xZn_{1-x}Se$ with zinc-blende structures higher than room temperature. Benstaali et al. [21] reported half-metallic FM phases in $Co_xZn_{1-x}Se$ which are in agreement with our results. Sirkeli and co-workers [22] investigated the magnetic properties of $Ni_xZn_{1-x}Se$ compounds with a Ni concentration of x=0.001-0.50 %. Ref. [22] studied the magnetic properties of the $Ni_xZn_{1-x}Se$ compound and predicted a half-metallic FM state. This result is closer to the theoretical predictions for $Ni_xZn_{1-x}Se$ (x=25%) as reported in Ref. [23].

2. CALCULATION METHOD

In this research, simulations were conducted using Density Functional Theory (DFT) with the Local Spin Density Approximation (LSDA) as the exchange-correlation functional [24,25], implemented in the Quantum ATK software (Atomistic ToolKit, http://quantumwise.com/) under a time-limited academic evaluation license provided by Synopsys. The software was used strictly in accordance with the licensing agreement for non-commercial academic research purposes. The fundamental equation in DFT is the Kohn-Sham equation [26], which results from the minimization of the total energy with respect to the electron density $\rho(r)$:

$$\left[-\frac{\hbar^2}{2m}\nabla^2 + V_{eff}(r)\right]\psi_i(r) = \varepsilon_i\psi_i(r). \tag{1}$$

Here, $\psi_i(r)$ and ε_i denote the wave functions and energies. The second term, V_{eff} in the brackets denotes the effective potential experienced by the electrons, and it is given:

$$V_{eff}(r) = V_{ext}(r) + V_{XC}(r) + V_H(r). \tag{2}$$

Here, V_{ext} denotes external potential due to the nuclei, V_{XC} denotes is the exchange-correlation potential derived from an approximate functional and V_{H} denotes the Hartree potential, which expressed by Equation (3):

$$V_H(r) = \int \frac{\rho(r')}{|r-r'|}dr'. \tag{3}$$

In DFT, the total energy functional expresses the total energy of an electronic system as a function of the electron density. It comprises several components: the kinetic energy of non-interacting electrons, the potential energy due to interactions between electrons and external potentials (e.g., nuclei), the classical electrostatic repulsion between electrons (Hartree energy), and the exchange-correlation energy, which

captures many-body quantum effects beyond classical interactions:

$$E[\rho] = T_s[\rho] + \int V_{ext}(r)\rho(r)dr + \frac{1}{2}\int \frac{\rho(r)\rho(r')}{|r-r'|}drdr' + E_{XC}[\rho]. \quad (4)$$

Here T_s denotes the kinetic energy of non-interacting electrons, while the $E_{XC}[\rho]$ and $\rho(r)$ represent the exchange-correlation energy and the electron density (5), respectively:

$$\rho(r) = \Sigma_i |\psi_i(r)|^2 . \quad (5)$$

The ferromagnetism for supercells at different impurity concentrations was investigated. In the LSDA research, the electron density is divided into two components such as majority (up, ρ^{α}) and minority spin (down, ρ^{β}). The total magnetization can be given by Equation (6):

$$M(r) = \rho^{\alpha}(r) - \rho^{\beta}(r). \quad (6)$$

In spin-polarized DFT-LSDA method, the exchange-correlation energy can be expressed by Equation (7):

$$E_{XC} = \int \rho(r)\varepsilon_{XC}(\rho^{\alpha}, \rho^{\beta})dr . \quad (7)$$

Recent advances using Hubbard U parameter [27] allow more accurate band gap predictions for materials. In this study, Hubbard U values of 4.5eV for zinc d-states, 3.8eV for selenium p-states were used [24, 26]. The correction follows the simplified Dudarev approach [27, 28], expressed as:

$$E_{DFT+U} = E_{DFT} + \frac{U_{eff}}{2}\sum_{A,\sigma}\sum_{m}\left[n_{mm}^{A\sigma} - \sum_{m'} n_{mm'}^{A\sigma} n_{m'm}^{A\sigma} \right]. \quad (8)$$

In the Dudarev approach, U_{eff} represents the effective on-site interaction. The $n_{mm'}^{A\sigma}$ is occupation matrix describes localized electronic orbitals m and m' on atom (A) with spin (σ), and the E_{DFT} denotes total energy of studied systems. These simulations were performed for various structures using lattice constants a=3.98 Å; c=6.53 Å [29]. Brillouin zone was sampled with a 5×5×5 Monkhorst-Pack grid (63 symmetry-reduced points), and atomic positions were fully optimized. A kinetic energy cutoff of 50 Ha was used and tested to ensure convergence.

Valence configurations used were: Zn +[Ar] $3d^{10}$ $4s^2$, Se +[Ar] $4s^2$ $4p^4$, Cr +[Ar] $3d^5$ $4s^1$, Fe +[Ar] $3d^6$ $4s^2$, and Ni +[Ar] $3d^8$ $4s^2$, where [Ar] denotes the argon core (first 18 electrons).

Mulliken population analysis [30] was used to calculate the magnetic moments in TM-doped ZnSe supercells. This method partitions the electron density among atoms and orbitals based on DFT results, providing atomic charges, bond populations, and spin-resolved electron distributions. In spin-polarized DFT, the difference between α- (↑) and β-spin (↓) populations on a given atom gives its local magnetic moment:

$$\mu = N_{\alpha}^{\uparrow} - N_{\beta}^{\downarrow}. \quad (9)$$

Here, N is the total number of all electrons. The projected density of states (PDOS) is calculated by expanding each discrete energy level using the Equation (10) [30], where the peaks represent one-electron

energies. Integrating the PDOS between energies E_1 to E_2 express the number of states. To enable visualization, δ-functions are broadened accordingly.

$$D^{\alpha}_{nl\sigma}(E) = \sum_i A^{\alpha}_{nl\sigma i} \frac{\delta/\pi}{(E-\varepsilon_{i\sigma})^2 + \delta^2}, \quad (10)$$

here $A^{\alpha}_{nl\sigma i}$ denotes the atomic orbital α. The TDOS is obtained by summing the partial DOS on atom α over all orbitals (n, *l*) and spin states (σ), as expressed in Equation (11):

$$D_{\sigma}(E) = \sum_{nl\alpha} D^{\alpha}_{nl\sigma}(E). \quad (11)$$

3. RESULTS AND DISCUSSION

3.1. Electronic Characteristics

Using Atomistic ToolKit code, we tested the band structure simulations for the pure ZnSe compound using different DFT methods. The DFT-LSDA simulation method is well known for underestimating the band gap of semiconductor materials, due to the inherent limitations of the LSDA functional. While LSDA typically yields deficient band gap values, more accurate results can often be achieved using hybrid functional or Hubbard U Coulomb interaction parameters, which provide more reliable corrections across a broad range of systems. However, recent advances of LSDA functionals and the use of semi-empirical Hubbard energy have enabled us to correct the limits of band gap limitation for materials. Note that we tested hybrid method for simulation of electronic band structure for ZnSe and this calculation takes more PC time than LSDA calculations.

First, we performed band structure calculations and obtained a band gap value of 1.57eV, which is significantly underestimated compared to the value of 2.7 eV measured from experiment [31] (Figure 1). Literature interpretations show that, the theoretically calculated band gap values for ZnSe reported in Ref. [1] and in Ref. [19] are significantly smaller than the experimentally determined value [31]. However, recent advances in the application of the Hubbard parametr have enabled us to estimate the bandgap of a 32-atom ZnSe supercell to be 2.7 eV, which is in close agreement with the experimental result [31].

The doping effect on the electronic structure and magnetic behaviors of ZnSe containing 32 and 64 atoms was investigated by substituting one and two Zn atoms with 3d transition metal atoms, respectively. The computed electronic structures and DOS curves for $Zn_{1-x}TM_xSe$ (x=12.5 %) are presented in Figures 2-7. TM is a transition metal, which will contribute localized d-states near the Fermi level. The blue lines in figures represent the local energy levels of TM atoms, particularly focusing on the regions near the Fermi energy level which might indicate either occupied or unoccupied electronic states. These figures illustrate the spin-up band structure of $Cr_xZn_{1-x}Se$, spin-down bands of $Fe_xZn_{1-x}Se$ and $Ni_xZn_{1-x}Se$ show half-metallic behavior: the some valence bands intersect the Fermi level, indicating the absence of a bandgap between the valence and conduction bands. Ref. [2] reported the majority spin gaps (1.42 eV; 1.66 eV) of $Cr_xZn_{1-x}Se$ with 6.25; 12.5 % and found underestimated band gap values than 2.88 and 3.01 eV. First- principles computed band gaps results for $Zn_{1-x}TM_xSe$ 32- and 64-atom supercells are listed in Table 1. As shown from this table, the spin-up bandgap for Cr-ZnSe and the spin-down bandgaps for Fe-ZnSe and Ni-ZnSe systems are zero, indicating metallic behavior in these spin channels and confirming that these compounds are half-metallic materials.

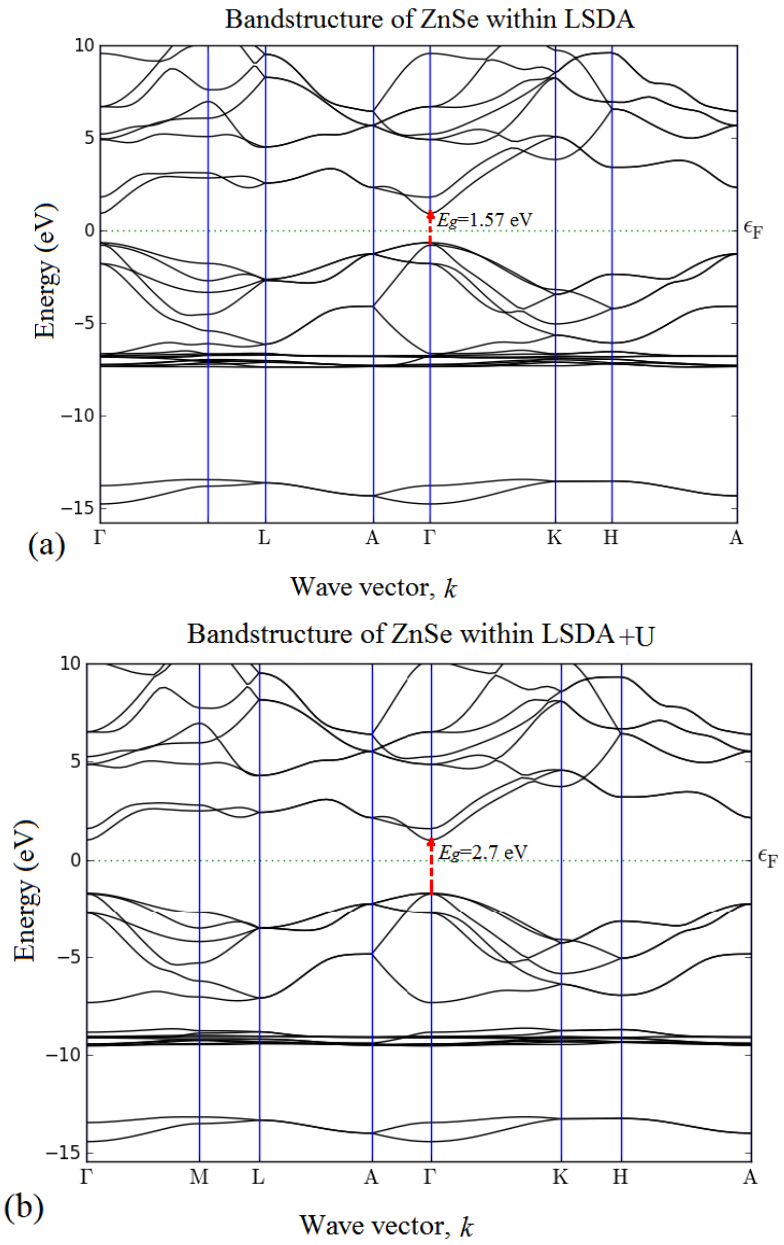

Figure 1. *DFT-LSDA* (a) *and LSDA+U* (b) *band structures for pure ZnSe*

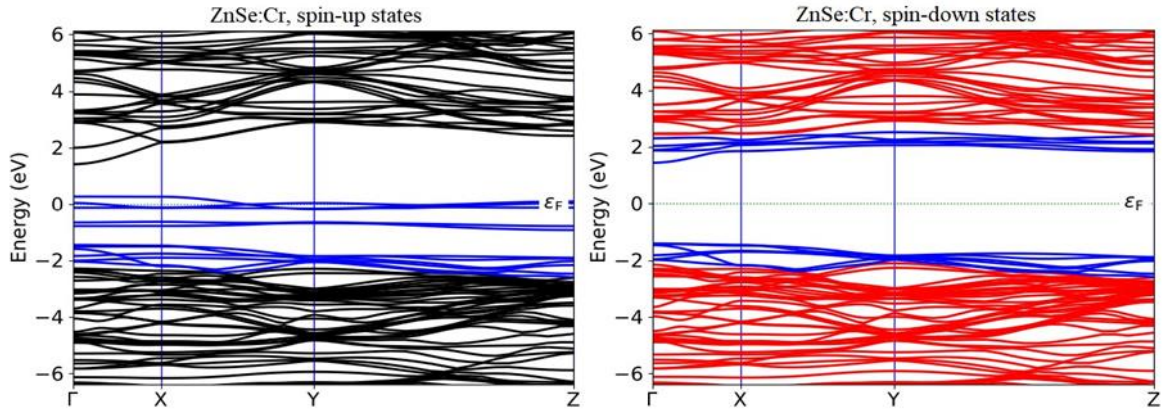

Figure 2. *Spin-up (on the left) and spin down (on the right) band structures for* $Cr_1Zn_{15}Se_{16}$*. The blue lines represent the local energy levels of Cr atoms near the Fermi level*

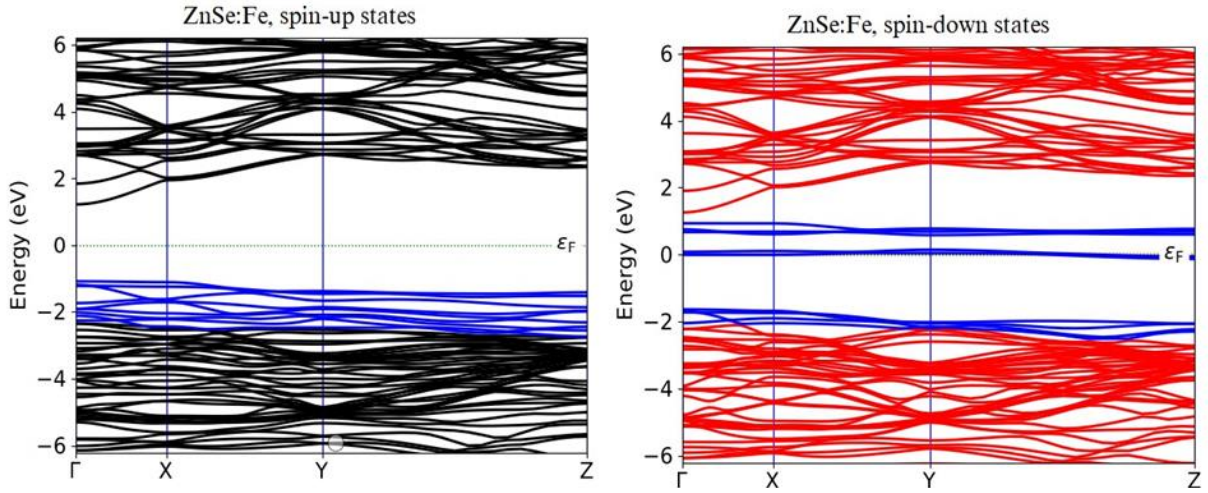

Figure 3. *Band structures for $Fe_1Zn_{15}Se_{16}$*

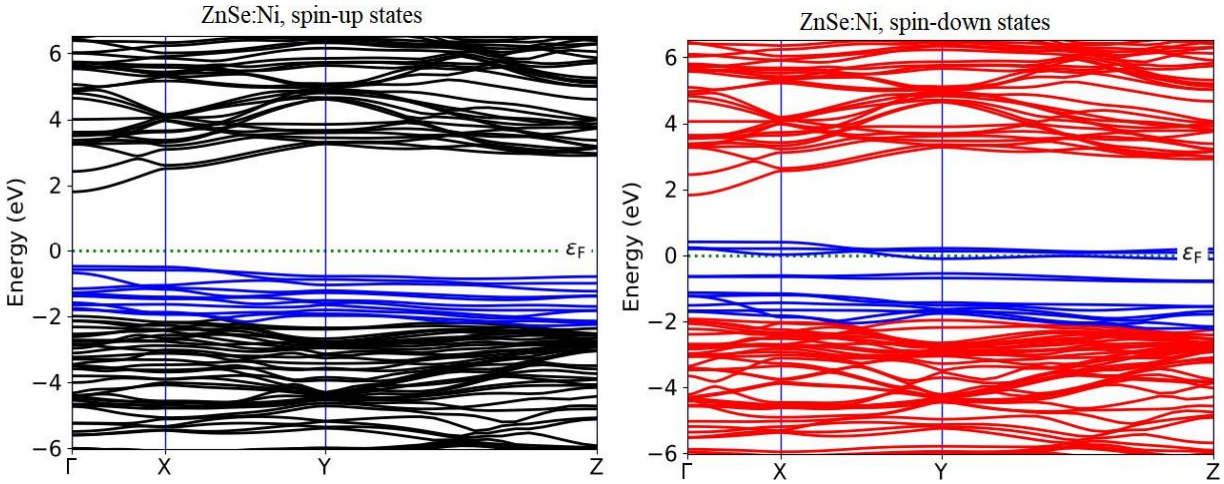

Figure 4. *Band structures for $Ni_1Zn_{15}Se_{16}$*

To clarify the mechanism behind spin-polarization in the DOS, we analyzed the TDOS for $TM_1Zn_{15}Se_{16}$ supercells, along with the partial DOS diagrams for the transition metal (TM) atoms and four neighboring Se atoms chemically bonding (CB) with metal atom are plotted in Figures 5-7. In these figures, the spin-up and spin-down DOS diagrams are represented by black and red curves. Significant imbalances and prominent new peaks are observed in the d-orbitals of the TM atoms near the Fermi energy (0 eV). Additionally, some degree of spin imbalance is also evident in the *p*-states of the dopants.

Table 1. *Bandgap results for $TM_xZn_{1-x}Se$ with impurity concentrations of 12.5 % and 6.25 %*

Supercells	*x*, %	Spin-up, eV	Spin-dn, eV
$Cr_1Zn_{15}Se_{16}$	6.25	0.0	2.8
$Fe_1Zn_{15}Se_{16}$	6.25	2.4	0.0
$Ni_1Zn_{15}Se_{16}$	6.25	2.5	0.0
$Cr_2Zn_{14}Se_{16}$	12.5	0.0	3.0
$Fe_2Zn_{14}Se_{16}$	12.5	2.2	0.0
$Ni_2Zn_{14}Se_{16}$	12.5	2.3	0.0
$Cr_2Zn_{30}Se_{32}$	6.25	0.0	2.9
$Fe_2Zn_{30}Se_{32}$	6.25	2.3	0.0
$Ni_2Zn_{30}Se_{32}$	6.25	2.4	0.0

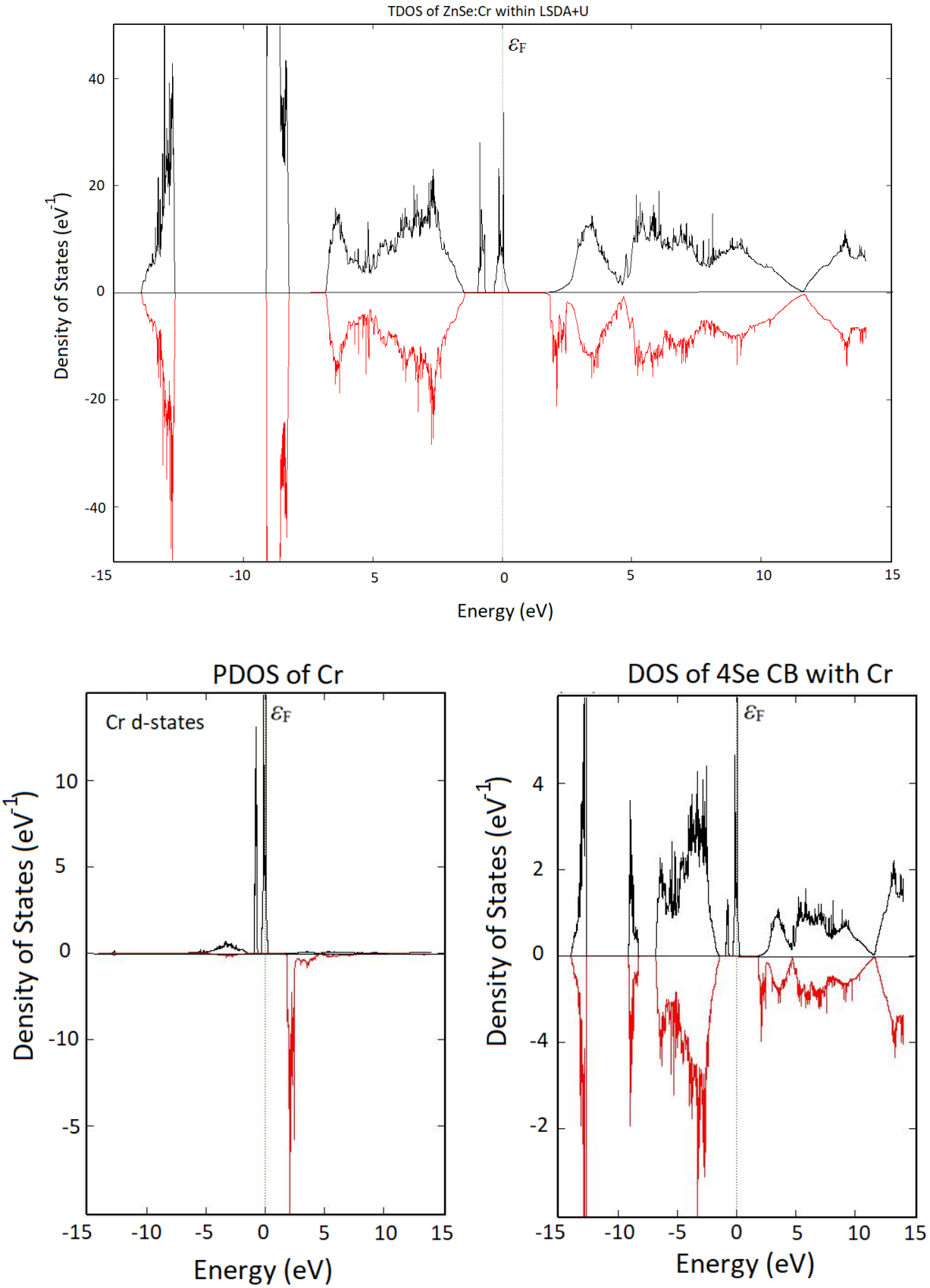

Figure 5. *DOS diagrams for $Cr_1Zn_{15}Se_{16}$ systems*

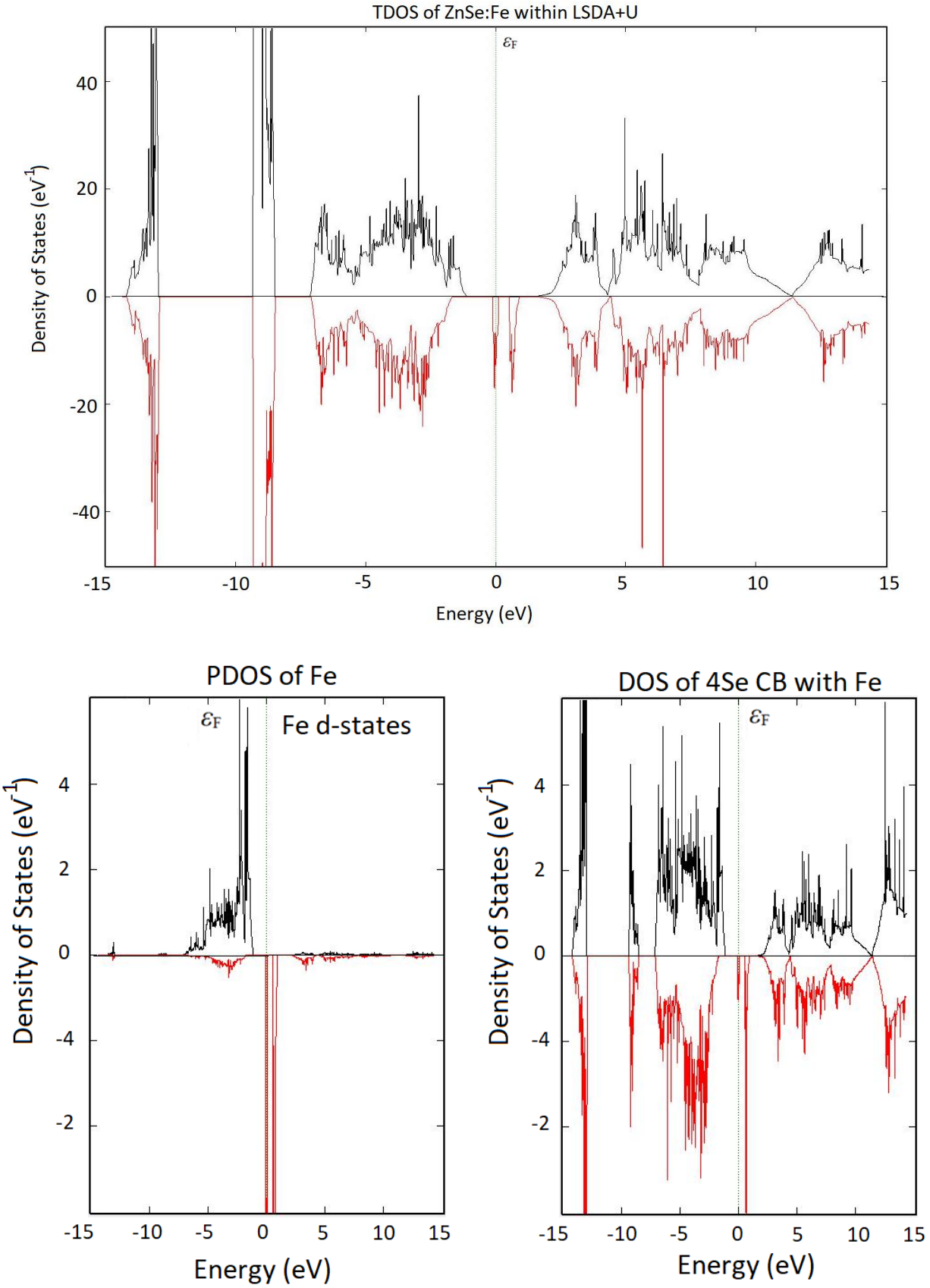

Figure 6. *DOS diagrams for $Fe_1Zn_{15}Se_{16}$ systems*

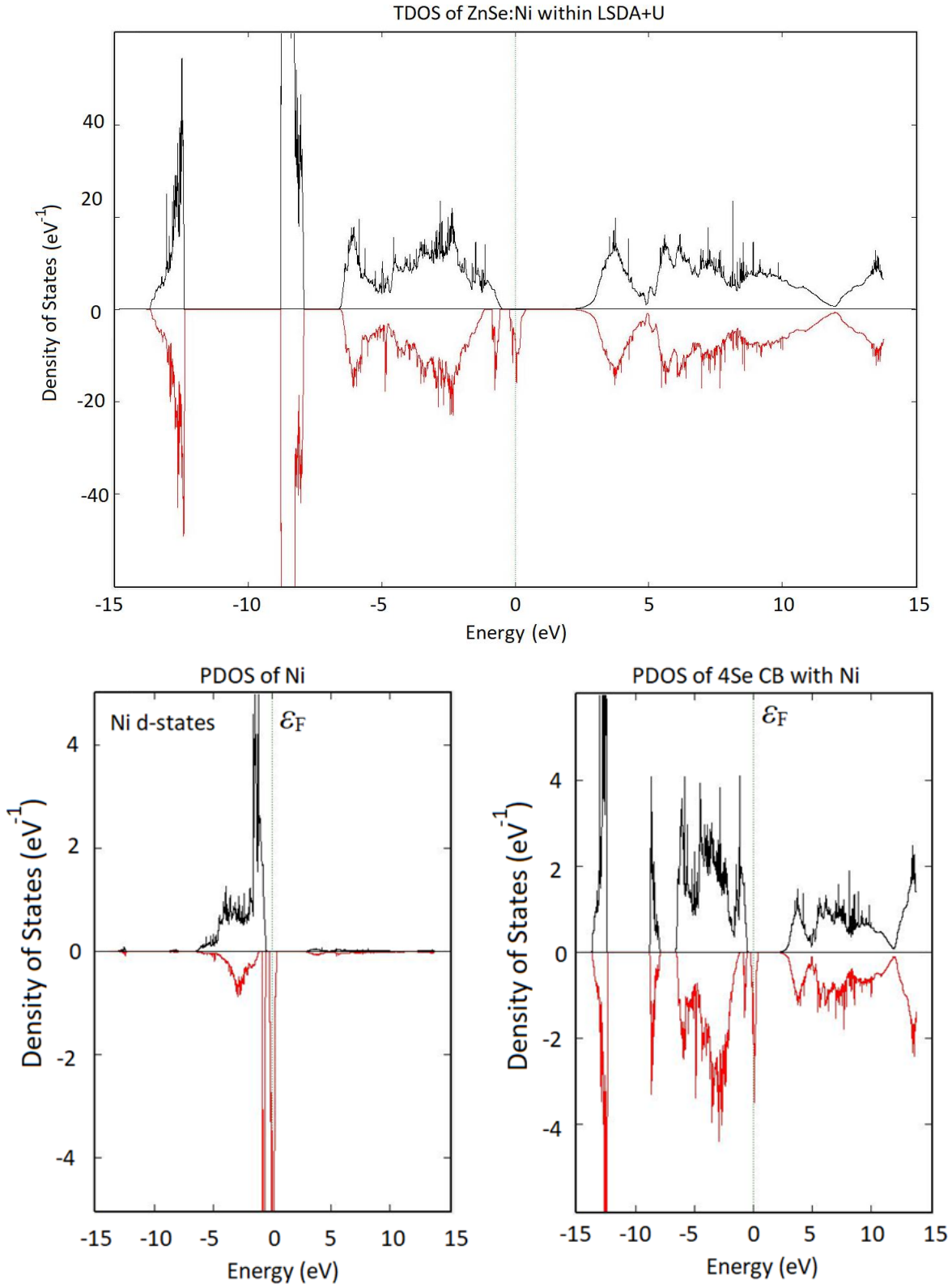

Figure 7. *DOS diagrams for $Ni_1Zn_{15}Se_{16}$ systems*

A systematic investigation of the electronic characteristics of the studied systems reveals that defective $Zn_{1-x}Cr_xSe$, $Zn_{1-x}Fe_xSe$, and $Zn_{1-x}Ni_xSe$ compounds exhibit half-metallic behavior. This is characterized by a metallic density of states in one spin channel and a semiconducting gap in the opposite spin channel, indicating strong spin-polarization behavior at the Fermi energy and potential suitability for technical applications.

3.2. Magnetism in $TM_xZn_{1-x}Se$

In computational studies, the energy difference between ferromagnetic and antiferromagnetic configurations provides insight into their relative stability. It is known that the total energy of system is significantly lower than another; it suggests that the lower-energy configuration is more favorable. The magnetic properties for investigated $TM_xZn_{1-x}Se$ systems were analyzed in detail implementing DFT+LSDA+U approach. Moreover, to obtain the stability of FM/AFM behaviors, the energy difference: $\Delta E = E_{AFM} - E_{FM}$ of defective systems, have been calculated. Table 2 presents the impurity concentrations; spin moments, the energy differences (ΔE) of both states for $Me_xZn_{1-x}Se$. From Table 2, our results predict that the magnetic moment of studied systems is ~4μ_B, and the value is independent of the impurity concentration. The total energy differences show FM phase stability of $TM_xZn_{1-x}Se$ supercells, this is closer to the results in Ref. [12].

Table 2. *The computed results for $TM_xZn_{1-x}Se$*

Supercell	*x*, %	μ,μ_B	ΔE, eV
$Zn_{14}Cr_2Se_{16}$	12.5	4.0	0.1018
$Zn_{30}Cr_2Se_{32}$	6.25	3.978	0.01148
$Zn_{14}Fe_2Se_{16}$	12.5	4.004	0.000215
$Zn_{30}Fe_2Se_{32}$	6.25	4.001	0.00002
$Zn_{14}Ni_2Se_{16}$	12.5	4.003	0.12004
$Zn_{30}Ni_2Se_{32}$	6.25	3.889	0.02328

In the ZnSe:TM supercell, magnetization is induced by the transition-metal dopants through the hybridization of selenium 4p orbitals with the dopant 3d orbitals. From first principles we obtained that the Cr doping ZnSe shows a slight change in magnetic moment between the two concentrations (12.5% vs 6.25%). As seen from Table 2, ZnSe:Fe has a magnetic moment close to 4 μ_B in both concentrations. Ni doping ZnSe exhibits a slight decrease in the magnetic moment (from 4.003 to 3.889 μ_B). Our results show that, the Fe doping seems to create the most stable configuration with minimal energy difference (ΔE) and a stable magnetic moment. Ni doping, on the other hand, might lead to weaker magnetism, with reduced magnetic moments and larger energy differences, indicating a less stable magnetic state (Figure 8).

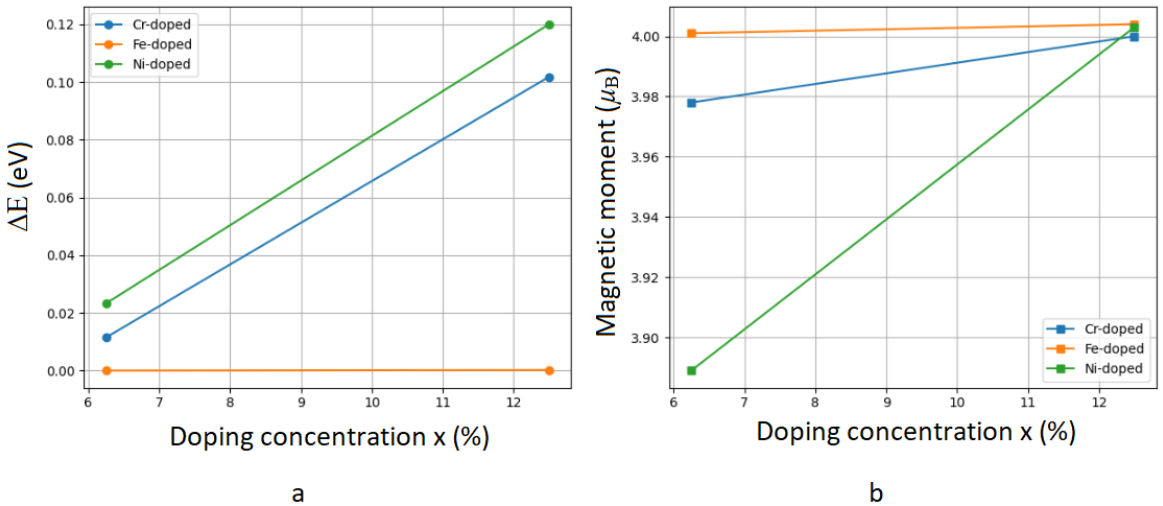

Figure 8. *(a) - energy difference (ΔE) and (b)-magnetic moment (μ) vs doping concentration (x)*

Figure 9 shows the spin-polarization view of $TM_1Zn_{15}Se_{16}$ and the black arrows describe the directions of local magnetic moments. The simulation results predict the magnetic moments in the defected systems originate primarily from the dopant d-orbitals, with only minor contributions from host atoms.

The consistent non-zero magnetic moments across the different compounds point to unfilled electronic

states in the conduction band, a trait often found in metallic systems. The small ΔE values indicate that there are not significant energy barriers for electron transitions, which is a criterion for metallic behavior. Comparing the results across different compounds with different impurity concentrations can provide insight into how the substitution impacts conductivity and magnetic properties. In our case, as seen in Table 2, the TM-doped ZnSe systems tend to exhibit higher magnetic moments suggesting a range of metallic behaviors. Based on the data presented in Table 2, we can deduce metallic behavior of the $TM_xZn_{1-x}Se$ systems through the presence of substantial magnetic moments and low energy separations. This feature generally correlates with the ability of the material to conduct electricity, affirming that the systems likely exhibit metallic characteristics, in the doped ZnSe with dopant atoms configurations, where the ΔE values approach zero.

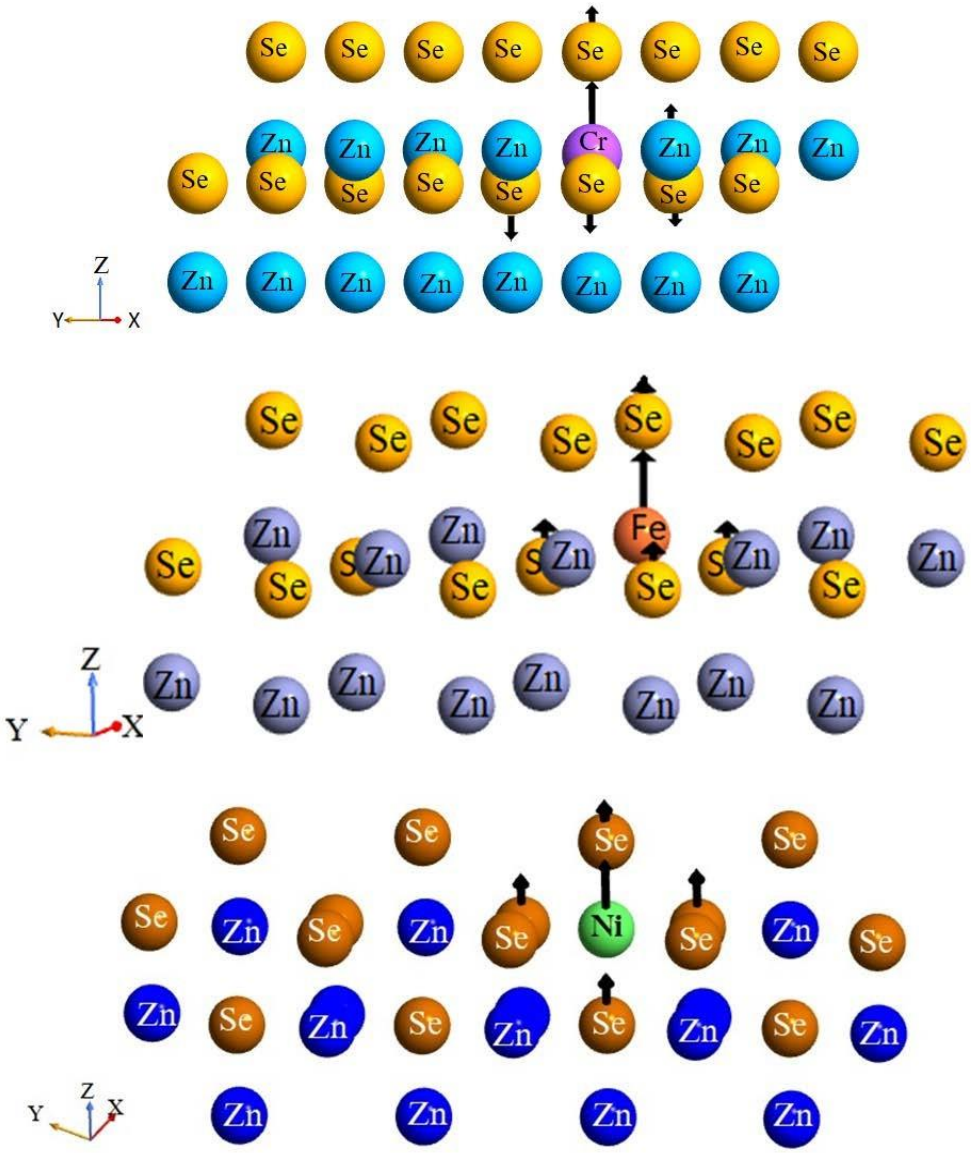

Figure 9. *Atomic structures and spin-polarization views of $TM_1Zn_{15}Se_{16}$ supercells doped with (top to bottom) Cr, Fe, and Ni*

On the other hand, we can provide insights into the bandgap of bulk solutions due to the obtained results for total energy differences for studied systems. From first-principles calculations, $Zn_{14}Cr_2Se_{16}$ (ΔE = 0.1018 eV) and $Zn_{30}Cr_2Se_{32}$ (ΔE = 0.01148 eV) systems show some energy separation but are relatively small, especially the latter. A small ΔE suggests that the material can have a metallic behavior, as it indicates narrow or nearly overlapping bands that can allow electron flow. In contrast, both $Zn_{14}Fe_2Se_{16}$ (Δ*E* = 0.000215 eV) and $Zn_{30}Fe_2Se_{32}$ (ΔE = 0.00002 eV) have very small energy separations, suggesting these systems have minimal band gaps and are likely metallic or exhibit half-metallic behavior, leading to good

conductivity. Additionally, $Zn_{14}Ni_2Se_{16}$ (ΔE = 0.12004 eV), while slightly higher, still indicates a low energy gap that suggests metallic behavior, especially when compared to typical semiconductors with larger band gaps. Depending on system's application (e.g., spintronic devices, magnetic materials), these results can be used to optimize dopant choice and concentration for achieving desired magnetic properties.

The magnetic moment for Cr in $Cr_xZn_{1-x}Se$ is estimated to be ~4.0 μ_B, with the main magnetization (~3.2 μ_B) coming from the *d*-states of the impurity. The magnetism of $Zn_{1-x}Cr_xSe$ is also influenced by smaller contributions: 15 Zn atoms contribute with a small value, and 16 Se atoms contribute with negative values of ~0.20, and -0.22 μ_B, respectively. The four selenium atoms chemically bonded to the dopant contribute negatively to the magnetization, resulting in a magnetic moment of approximately -0.6μ_B. The computed magnetic moment for the $Zn_{1-x}Cr_xSe$ is 4.0μ_B, which aligns well with the values reported in Ref. [2], where magnetic moments of ~3.98 μ_B and ~3.99 μ_B were obtained for the $Cr_2Zn_6Se_8$ and $Cr_2Zn_{14}Se_{16}$ compounds, respectively. These results from Ref. [2] were derived from Full-Potential Linear Muffin-Tin-Orbital approach, supporting the reliability of our findings.

From first-principles research, the spin moment for $Fe_xZn_{1-x}Se$ is around ~4μ_B. This result is consistent with results of approximately 4.8μ_B found in Ref. [32] for the $Fe_xZn_{1-x}Se$ nanosheet. In Fe substituting for Zn, the zinc atoms exert only a minor demagnetizing effect on the system, contributing approximately -0.05 μ_B. The overall magnetization in the $Fe_xZn_{1-x}Se$ is primarily attributed to the Fe dopant, with a total spin moment of about 3.5 μ_B, of which 3.3 μ_B originates from the Fe *d*-electrons. The primary contributions to the magnetization of $Zn_{1-x}Fe_xSe$ arise from the four selenium atoms bonded to Fe dopant, which have a total magnetic moment of μ=0.7 μ_B. In the case of $Ni_xZn_{1-x}Se$, the magnetic moments for the defective systems and the Ni dopant were estimated to be approximately 4.0 μ_B and 1.2 μ_B. A significant contribution of about 1.2 μ_B to the overall magnetization originates from the d-electrons of the nickel dopant, while the 15 surrounding zinc atoms contribute small negative spin moments. Additionally, the four selenium atoms that are chemically bonded to nickel contribute approximately 0.8 μ_B to the total magnetization.

3.3. Curie Temperature for $TM_xZn_{1-x}Se$

The Curie temperature (T_C) is a key parameter in the study of ferromagnetism, as it reflects the overall strength of inter-sublattice magnetic interactions in a material. In this study, Curie temperatures of $Fe_xZn_{1-x}Se$, $Cr_xZn_{1-x}Se$, and $Ni_xZn_{1-x}Se$ defective compounds with dopant concentrations of x = 6.25% and 12.5%were estimated using the Mean Field Approximation method, as described in Ref. [33, 34]

$$T_C = \frac{2}{3}\frac{\Delta E}{k_B x}. \tag{13}$$

In this expression, k_B is the Boltzmann constant, x is the impurity concentration, and ΔE denotes the total energy difference between the antiferromagnetic (AFM) and ferromagnetic (FM) behaviors. Curie temperatures (T_C) for $TM_xZn_{1-x}Se$ bulk alloys are estimated and tabulated in Table 3.

The work [12] predicted Curie temperature higher than room temperature for $Cr_xZn_{1-x}Se$ and $Ni_xZn_{1-x}Se$, and our results are closer to Ref. [12]. From *ab initio* simulations, the T_C decreases with the decreasing of concentrations of dopants for all $TM_xZn_{1-x}Se$ systems. Our simulations indicate that $Cr_xZn_{1-x}Se$ and $Ni_xZn_{1-x}Se$ exhibit metallic character and Curie temperatures above 300 *K*, suggesting their potential suitability for spintronic device applications. The $Fe_xZn_{1-x}Se$ exhibit relatively low Curie temperatures, indicating a paramagnetic ground state. Despite this, their properties make them promising candidates for optoelectronic applications.

Table 3. *The first-principles results for $TM_xZn_{1-x}Se$*

Supercells Compound	*x*, %	ΔE [eV]	T_C, K

$Zn_{14}Cr_2Se_{16}$	12.5	0.1018	3150
$Zn_{14}Fe_2Se_{16}$	12.5	0.000215	25
$Zn_{14}Ni_2Se_{16}$	12.5	0.12004	3714
$Zn_{30}Cr_2Se_{32}$	6.25	0.01148	711
$Zn_{30}Fe_2Se_{32}$	6.25	0.00002	5
$Zn_{30}Ni_2Se_{32}$	6.25	0.02328	1440

4. CONCLUSION

We analyzed the electronic and magnetic characteristics for $TM_xZn_{1-x}Se$ bulk solutions (with TM = Cr, Fe, Ni) at dopant concentrations of 6.25% and 12.5% using the LSDA combined with Hubbard U semiempirical Coulomb interaction corrections. The incorporation of 3d transition metals into ZnSe supercells significantly modified the electronic structure; inducing half-metallic behavior in the $TM_xZn_{1-x}Se$ diluted magnetic semiconductors. According to our simulations, the calculated spin moments are ~4.0μ_B for $Zn_{1-x}Cr_xSe$, $Zn_{1-x}Ni_xSe$, and ~5.0μ_B for $Zn_{1-x}Fe_xSe$. The dominant contribution to the total magnetization arises from the d-orbitals of the 3d transition metal dopants. Total energy results further predict that the ferromagnetic phase is energetically favorable for all three systems. The current results predicted that the magnetization of $TM_xZn_{1-x}Se$ systems is dependent on the concentrations of impurities, and $Cr_xZn_{1-x}Se$ and $Ni_xZn_{1-x}Se$ are higher Curie temperature ferromagnetic materials with half-metallic character, and the $Fe_xZn_{1-x}Se$ exhibit paramagnetic behavior, making them promising candidates for optoelectronic applications.

Our simulations predicted that chromium- and nickel-doped ZnSe compounds are potential candidates for spin valve devices.

CONFLICTS OF INTEREST

No conflict of interest was declared by the authors.

REFERENCES

[1] Dai, S., Feng, G., Zhang, Y., Deng, L., Zhang, H., and Zhou, S., "The effects of the impurity distribution on the electrical and optical properties of Cr^{2+}: ZnSe nanowires: First-principles study", Results in Physics, 8: 628, (2018).

[2] Cheref, O., Dahmane, F., Benalia, S., Rached, D., Mokhtari, M., Djoudi, L., Merabet, M., and Bettahar, N., "First-principles study of half-metallic properties in X_2VSi (X = Ti, Co) and their quaternary TiCoVSi and CoTiVSi compounds", Computational Condensed Matterials, 19: e00369, (2019).

[3] Wolf, S.A., Awschalom, D.D., Buhrman, R.A., Daughton, M., von Molnar, S., Roukes, M.L., Chtchelkanova, A.Y., and Treger, D.M., "Spintronics: a spin-based electronics vision for the future", Science, 294: 1488, (2001).

[4] Liu, C., Yun, F., Morkoc, H., "Ferromagnetism of ZnO and GaN: A Review", Journal of Materials Science: Materials in Electronics, 16: 555, (2005).

[5] Pickett, W.E., Moodera, J.S., "Half Metallic Magnets", Physics Today, 54(5): 39, (2001).

[6] Sato, K., Katayama-Yoshida, H., "Materials Design of Transparent and Half-Metallic Ferromagnets in V- or Cr-Doped ZnS, ZnSe and ZnTe without P- or N-type Doping Treatment", Journal of Applied Physics, 40: L651, (2001).

[7] Wu, S.Y., Liu, H.X., Gu, L., Singh, R.K., Budd, L., van Schilfgaarde, M., McCartney, M.R., Smith, D.J., Newman, N., "Synthesis, characterization, and modeling of high quality ferromagnetic Cr-doped AlN thin films", Applied Physics Letters, 82: 3047, (2003).

[8] Mokaddem, A., Doumi, B., Sayede, A., Bensaid, D., Tadjer, A., and Boutaleb, M., "Investigations of electronic structure and half-metallic ferromagnets in Cr-doped zinc-blende BeS semiconductor", Journal of Superconductivity and Novel Magnetism, 28: 157, (2015).

[9] Behloul, M., Salmani, E., Ez-Zahraouy, H., and Benyoussef, A., "Theoretical investigation of electronic, magnetic and optical properties of ZnSe doped TM and co-doped with MnTM (TM: Fe, Cr, Co): AB-initio study", Journal of Magnetism and Magnetic Materials, 419: 233, (2016).

[10] Stern, R.A., Schuler, T.M., MacLaren, J.M., Ederer, D.L., Perez-Dieste, V., and Himpsel, F.J., "Calculated half-metallic behavior in dilute magnetically doped ZnS", Journal of Applied Physisc, 95: 7468-7470, (2004).

[11] Blinowski, J., Kacman, P., and Majewski, J.A., "Ferromagnetic superexchange in Cr-based diluted magnetic semiconductors", Physical Review B, 53: 9534, (1996).

[12] Sato, K., Katayama-Yoshida, H., "Ab initio study on the magnetism in ZnO-, ZnS-, ZnSe-and ZnTe-based diluted magnetic semiconductors", Physica Status Solidi (b), 229: 673, (2002).

[13] Saito, H., Zaets, V., Yamataga, S., Suzuki, Y., and Ando, K., "Ferromagnetism in II–VI diluted magnetic semiconductor $Zn_{1-x}Cr_xTe$", Journal of Applied Physics, 91(10): 8085-8087, (2002).

[14] Maksimov, V.I., Dubinin, S.F., and Surkova, T.P., "Superstructure of atomic displacements in cubic compounds $Zn_{0.9}Ni_{0.1}S$ and $Zn_{0.7}Ni_{0.3}O$", Physica Solid State, 56: 2393, (2014).

[15] Ge, X.F., Zhang, Y.M., "First-principles study of half-metallic ferromagnetism in $Zn_{1-x}Cr_xSe$", Journal of Magnetism and Magnetic Materials, 321(3): 198-202, (2009).

[16] Serre, H., Basterd, G., Rigaux, C., Mycielski, J., and Furdyna, J.K., "Proc. Int. Conf. Phys. of Narrow- Gap Semicond. Linz 1981", Lecture Notes in Physics, Springer, Berlin, 152: 321, (1982).

[17] Furdyna, J.K., "Diluted magnetic semiconductors", Journal of Applied Physics, 64: K29-K64б, (1988).

[18] Katayama-Yoshida, H., Sato, K., "Spin and charge control method of ternary II–VI and III–V magnetic semiconductors for spintronics: theory vs. Experiment", Journal of Physics and Chemistry of Solids, 64: 1447, (2003).

[19] Khan, M.Sh., Shi, L., and Zou, B., "Impact of vacancy defects on optoelectronic and magnetic properties of Mn-doped ZnSe", Computational Materials Science, 174: 109493, (2020).

[20] Jafarova, V.N., "Ab-initio calculation of structural and electronic properties of ZnO and ZnSe compounds with wurtzite structure", International Journal of Modern Physics B, 36(24): 2250156-1-13, (2022).

[21] Benstaali, W., Bentata, S., Abbad, A., and Belaidi, A., "Ab-initio study of magnetic, electronic and optical properties of ZnSe doped-transition metals", Materials Science in Semiconductor Processing, 16: 231, (2013).

[22] Sirkeli, V., Radevici, I., Sushkevich, K., Huhtinen, H., Nedeoglo, N., Nedeoglo, D., Paturi, P., "Magnetic and luminescent properties of nickel-doped ZnSe crystals", Solid State Sciences, 5: 74-80, (2015).

[23] Khan, M.Sh., Shi, L., Ullah, H., Yanga, X., and Zou, B., "Ab initio study of optoelectronic and magnetic properties of Mn-doped ZnS with and without vacancy defects", Journal of Physics: Condensed Matter, 31: 485706, (2019).

[24] Jafarova, V.N., Scurtu, I.C., Stanca, C., Acomi, N., and Raicu, G., "Defect influence on the electronic and magnetic properties of silver-doped (6,0) single-walled ZnO nanotubes: a first-principles study", Indian Journal of Physics, 98: 2335-2346, (2024).

[25] Jafarova, V.N., "High Curie temperature and half-metallic ferromagnetism in Cr- and V-doped ZnSe in wurtzite phase: First-principles study", Solid State Communications, 369: 115197, (2023).

[26] Kohn, W., Sham, L.J., "Self-Consistent Equations Including Exchange and Correlation Effects", Physical Review A, 140: 1133-1138, (1965).

[27] Cococcioni, M., de Gironcoli, S, "Linear response approach to the calculation of the effective interaction parameters in the LDA+U method", Physical Review B, 71:035105, (2005).

[28] Dudarev, S.L., Botton, G.A., Savrasov, S.Y., Humphreys, C.J., and Sutton, A.P., "Electron-energy-loss spectra and the structural stability of nickel oxide: An LSDA+U study", Physical Review B, 57: 1505, (1998).

[29] Liechtenstein, A.I., Anisimov, V.I., and Zaanen, J., "Density-functional theory and strong interactions: Orbital ordering in Mott-Hubbard insulators", Physical Review B, 52: R5467, (1995).

[30] Wyckoff, R.W.G., "Crystal Structures", Second Edition, John Wiley and Sons, 1: 85, (1963).

[31] North, S.C., Jorgensen, K.R., Pricetolstoy J., and Wilson, A.K., "Population analysis and the effects of Gaussian basis set quality and quantum mechanical approach: main group through heavy element species", Frontiers in Chemistry, 11: 1152500, (2023).

[32] Theis, D., "Wavelength-modulated reflectivity spectra of ZnSe and ZnS from 2.5 to 8 eV", Physica Status Solidi (b), 79(1): 125-130, (1977).

[33] Chen, X.L., Huang, B.J., Feng, Y., Wang, P.J., Zhang C.W., and Li, P., "Electronic structures and optical properties of TM (Cr, Mn, Fe or Co) atom doped ZnSe nanosheets", RSC Advances, 5: 106227, (2015).

[34] Jafarova, V.N., "Structural, electronic and magnetic properties of pure and Fe-doped ZnSe: first principles investigation", Pramana – Journal of Physics, 98: 82, (2024).